Detectability of nondifferentiable generalized synchrony

Nikolai F. Rulkov[1] and Valentin S. Afraimovich[2]
[1]*Institute for Nonlinear Science, University of California, San Diego, La Jolla, California 92093-0402, USA*
[2]*Instituto de Investigación en Communicación Optica, Universidad Autónoma de San Luis Potosí, San Luis Potosí, Mexico*
(Received 16 October 2002; revised manuscript received 23 April 2003; published 27 June 2003)

Generalized synchronization of chaos is a type of cooperative behavior in directionally coupled oscillators that is characterized by existence of stable and persistent functional dependence of response trajectories from the chaotic trajectory of driving oscillator. In many practical cases this function is nondifferentiable and has a very complex shape. The generalized synchrony in such cases seems to be undetectable, and only the cases in which a differentiable synchronization function exists are considered to make sense in practice. We show that this viewpoint is not always correct and the nondifferentiable generalized synchrony can be revealed in many practical cases. Conditions for detection of generalized synchrony are derived analytically, and illustrated numerically with a simple example of nondifferentiable generalized synchronization.

DOI: 10.1103/PhysRevE.67.066218 PACS number(s): 05.45.Xt, 05.45.Tp

I. INTRODUCTION

Synchronization plays an important role both for understanding of cooperative behavior in natural networks of oscillators [1] and for various engineering applications [2,3]. Recently, a significant interest in understanding and giving theoretical description of synchronization regimes, among the oscillators with chaotic behavior, is perceived; see, for example, recent books and reviews [4–6]. Various types of chaos synchrony, whose description may require different theoretical frameworks, were found in natural systems and specified. These types of synchrony include identical synchronization [7–9], generalized synchronization [10–13], and phase synchronization [14,15].

The framework of generalized synchronization was proposed as an attempt to extend the classical theory of forced synchronization of a periodic oscillator, initiated by the works of van der Pol [16] and Andronov and Witt [17], to the case of directionally coupled chaotic oscillators. This framework defines synchronization as the onset of conditional stability of a chaotically driven oscillator and as the existence of a functional relation that maps the chaotic trajectory of driving oscillator into the trajectory of driven oscillator [10,18]. In the case of invertible dynamics of the driving system, such functional relation is usually substituted with a function that maps the state of the driving system into the state of response when these states are measured simultaneously. Rigorous mathematical results indicate that, depending on the strength of conditional stability, the synchronization function can be differentiable or nondifferentiable [19–23]. In many experimental studies, the researcher needs to establish the fact of chaos synchronization when direct analysis of conditional stability is hardly possible. In such a situation, the detection of generalized chaos synchrony characterized by a nondifferentiable function, which due to dense wrinkles, cusps, and finite number of points appears as a thick and fuzzy set, may seem to be impossible [20,24,25].

In this paper we show that detectability of the nondifferentiable synchrony can be significantly improved and become feasible if one explores synchronization function, taking into account additional points on sufficiently long intervals of the driving trajectory preceding the current state. The paper is organized as follows. In Sec. II we discuss the idea of such detectability and evaluate the improvement using numerical analysis of a simple example. Section III develops a theoretical argument explaining the mechanism behind the detectability improvement. Section IV discusses possible effects caused by small additive noise in the data. Summary of the results and possible applications are discussed in the Conclusion.

II. NUMERICAL EXAMPLE

To illustrate the idea of detectability enhancement, we first consider an example of a drive-response system which was proposed and studied in Ref. [20]. In this example, generalized baker map

$$x_{n+1}^{(1)}=\begin{cases}\lambda_a x_n^{(1)} & \text{if } x_n^{(2)}<a\\ \lambda_a+\lambda_b x_n^{(1)} & \text{if } x_n^{(2)}\geqslant a,\end{cases} \tag{1a}$$

$$x_{n+1}^{(2)}=\begin{cases}x_n^{(2)}/a & \text{if } x_n^{(2)}<a\\ (x_n^{(2)}-a)/b & \text{if } x_n^{(2)}\geqslant a,\end{cases} \tag{1b}$$

where $0\leqslant x_n^{(i)}<1$, $\lambda_a=1-\lambda_b=0.3$, and $a=1-b=0.5$ drives a system of the form

$$y_{n+1}=cy_n+\cos(2\pi x_n^{(1)}). \tag{2}$$

Here parameter c defines the properties of the response behavior. Consider the system dynamics within the parameter interval $0<c<1$. In this case, response system (2) is conditionally stable. The dynamics of driving system (1) is invertible, and according to the theory (see, for example, Refs. [22,23]) there exists a continuous function $y_n=h(\mathbf{x}_n)$, where $\mathbf{x}_n=(x_n^{(1)},x_n^{(2)})$. Due to the specific form of the driving and response systems, function h, in our case, is independent of $x_n^{(2)}$. Indeed, given the value of $x_n^{(1)}$, all previous values of this variable can be found from Eq. (1a), when one iterates this one-dimensional map backward in time, and these values

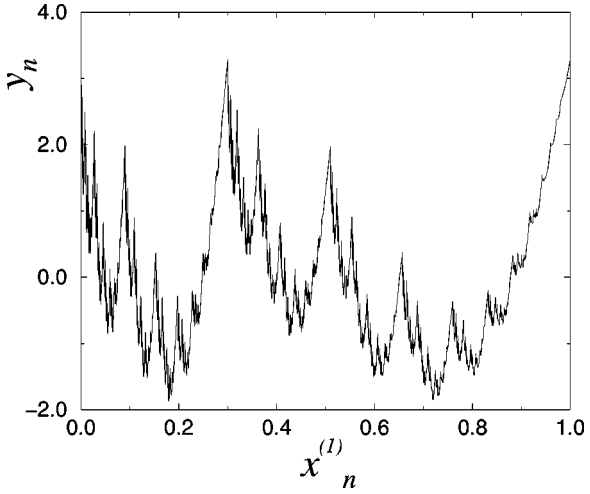

FIG. 1. The shape of the function $y_n = h(x_n^{(1)})$ computed with $c = 0.7$.

are independent of $x_n^{(2)}$. Therefore, function h can be plotted as a graph in the variables plane $(x_n^{(1)}, y_n)$.

The example of nondifferentiable function h, computed with $c = 0.7$, is shown in Fig. 1. It is clear from the shape of the function that, in a practical situation with a similar function, the existence of the function cannot be revealed from such a plot because the states of response system measured for nearby states of the driving system can be very disperse. This situation can lead one to believe that the onset of nondifferentiable generalized synchronization is practically undetectable. The statements on such practical undetectability are usually made when one analyses only relation between simultaneous states in the attractors of the driving and response systems. One may ask if additional information about the chaotic trajectory can help to resolve the complexity of this functional relation? And if the answer is yes, which properties of the nondifferentiable function can be improved?

To illustrate a positive answer to the first question, we adopt the approach developed in Ref. [26] and consider the additional information about the driving chaotic trajectory $\mathbf{x}_n$, using its symbolic description. Now we define the state of the driving system as the value of $x_{n-m}^{(1)}$ and the symbolic sequence $[\alpha_1, \ldots, \alpha_m]$ generated in the next consecutive iterations towards $x_n^{(1)}$. In the considered example, symbols α_i can be easily defined from the evolution of variable $x_n^{(2)}$. If $x_{n-i}^{(2)} < a$, then $\alpha_i = 0$. If $x_{n-i}^{(2)} \geqslant a$, then $\alpha_i = 1$. From the data generated by the maps (1) and (2) we can examine synchronization function in a new form $h^{(m)}$ which is defined as a mapping $([\alpha_1, \ldots, \alpha_m], x_{n-m}^{(1)}) \rightarrow y_n$.

In order to illustrate the improvement of the modified synchronization function $h^{(m)}$ with the increase of m, we plot y_n vs $([\alpha_1, \ldots, \alpha_m], x_{n-m}^{(1)})$ for two fixed symbolic sequences that differ by two most recent symbols. The cases of $m = 4$ and $m = 8$ are presented in Figs. 2(a) and 2(b) respectively, where the parameters of the maps are the same as in Fig. 1. Comparing these plots with the plot shown in Fig. 1 one can see that the existence of synchronization function becomes more apparent as the delay m increases. Notice that the scales of corresponding axes in these plots are the same.

We studied how the complex image of synchronized attractors in the space of a drive-response system converges to a ''good'' simple function with the increase of m. We analyzed the sets of attractor points conditioned by all possible symbolic masks of various lengths m. For each mask of preceding symbols $S_m^i = [\alpha_1, \ldots, \alpha_m]$ we computed the best polynomial fitting function $\phi_{S_m^i}(x)$ of order 30, using the Singular Value Decomposition algorithm, and studied the dependence of mean squared error (E_{MS}), averaged over all masks of length m, on the value of m. This dependence, computed for four different values of c, is shown in Fig. 3.

One can see from Fig. 3 that E_{MS} decreases exponentially fast when m increases. Approximating this dependence with exponential

$$E_{MS}(m) \sim e^{\Lambda m}, \tag{3}$$

one can find the rate of convergence Λ. Figure 4 shows how the convergence rate Λ evolves with the change of parameter

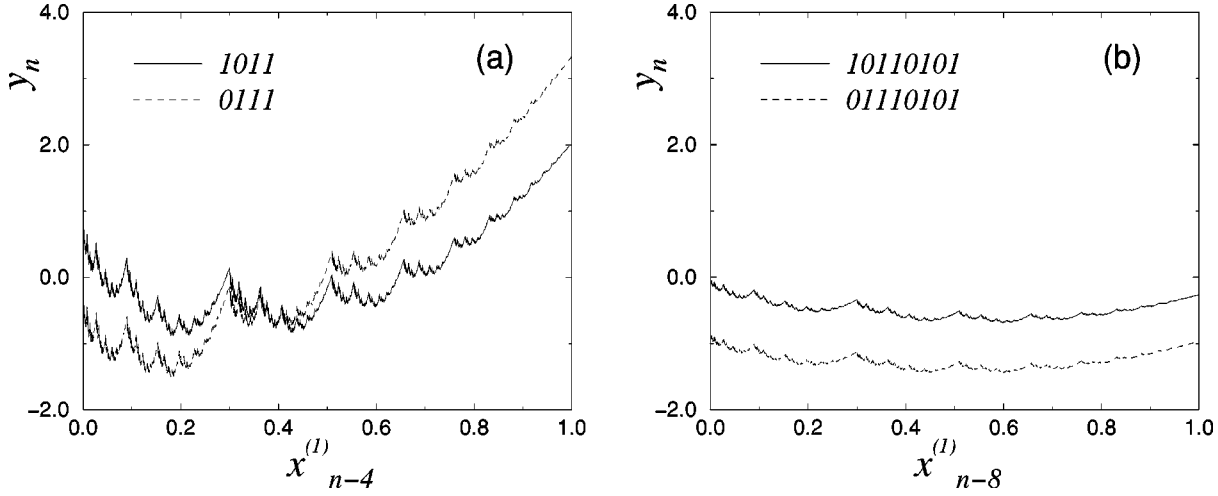

FIG. 2. The synchronization function computed using additional symbolic information on the driving trajectory for the case shown in Fig. 1. Only two symbolic masks, each of length m, are presented. The case $m = 4$ is shown in panel (a) and $m = 8$ is in panel (b).

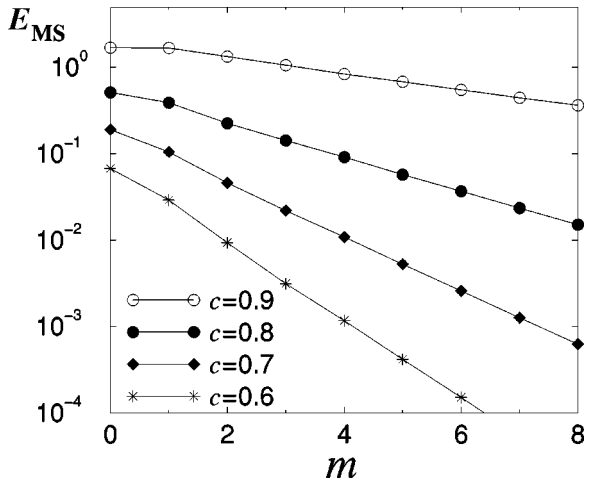

FIG. 3. The dependence of mean squared error of best polynomial fitting function for the attractor points (x_{n-m},y_n) on length m of the preceding masks S_m^i.

value c. The absolute value of Λ decreases as the value of c grows. This indicates that for higher values of c, the synchronization function becomes more complex [20] and its detection, with a given resolution, requires more information on the driving trajectory than for lower values of c.

One can easily check that when $c\to 1$, the conditional dynamics of response system (2) approaches the threshold of instability and, as the result, synchronization terminates and function h disappears. The plot of Λ vs c reflects this fact and one can see from Fig. 4 that convergence rate Λ tends to zero as $c\to 1$. It can be shown that the linear dependence of Λ on $\log(c)$ is due to the fact that the response system in this example is a linear system and $\log(|c|)$ is the contraction rate of its phase volume.

To get a better view on the function improvement, examine how additional symbolic information collected along the driving trajectory changes the shape of the whole synchronization function. One way of taking such symbolic information into account is to compute the integer value out of binary symbolic mask S_m^i and, then, supplement this integer with the fractional value given by $x_{n-m}^{(1)}$. Note that in our case $0\leqslant x_{n-m}^{(1)}<1$. Computing the integer part, we assume that the most recent symbol α_1 of mask S_m^i is the most significant bit. As a result, we obtain the decimal values of the form $I(S_m^i)\cdot x_{n-m}^{(1)}$. Every decimal value is considered as a new argument of the modified synchronization function $h^{(m)}$. Figure 5 presents such a function, plotted for three different values of m. One can see that for large m $(m>4)$, the overall shape and complexity of the function remains about the same, but the interval of the argument increases in size by a factor of 2^m. This indicates that there exists some kind of self-similarity of the nondifferentiable synchronization function, and the enhanced detectability is the result of more precise evaluation of the state of the driving system. It is important to note that the precision of the state evaluation increases with m, despite the fact that the values of variable $x^{(1)}$ are measured with the same precision as before.

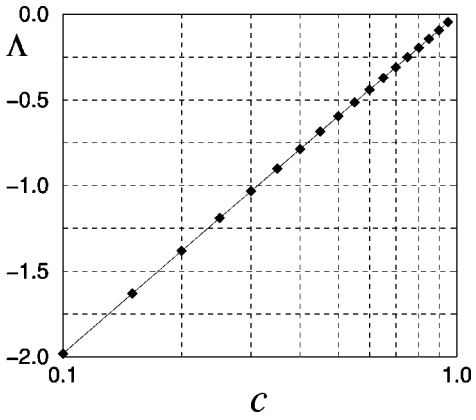

FIG. 4. The dependence of convergence rate Λ on the value of coupling parameter c, plotted in the logarithmic scale.

III. THEORETICAL RESULTS

The example considered above clearly indicates that the functional relation between the synchronized system becomes more apparent when the length of the driving trajectory, taken for the analysis, increases. In order to examine which properties of the nondifferentiable function change, and simplify the detection of the functional relation, we present the following theoretical analysis.

In this section we shall concentrate on systems with a unidirectional coupling (or systems with a skew product structure) of the form

$$x'=f(x),$$
$$y'=g_\rho(x,y). \tag{4}$$

These equations determine a map $F_\rho:(x,y)\mapsto(x',y')$, generating a dynamical system. The first subsystem is called the driving system, the second subsystem is called the response system and ρ is a parameter that controls the coupling strength. The fact of synchronization in this systems, means that there is a region of parameter values ρ in which, for any initial condition (x_0,y_0), $(x_0,\tilde{y}_0)$,

$$\lim_{n\to\infty} d(y_n,\tilde{y}_n)=0, \tag{5}$$

where $(x_n,y_n)=F_\rho^n(x_0,y_0)$ $[(x_n,\tilde{y}_n)=F_\rho^n(x_0,\tilde{y}_0)]$ and $d(y_n,\tilde{y}_n)$ is a distance in the phase space between y_n and $\tilde{y}_n$. Loosely speaking, this means that, for any initial condition, the distance between the states of the slave subsystem goes to zero with time.

We assume, for the sake of definiteness, that in system (4) one has $x\in\mathbb{R}^d$ and $y\in\mathbb{R}^\ell$, and that g_ρ is continuous and f is a homeomorphism. Since we study dissipative systems, we also assume that there exists a ball of dissipation $B\subset\mathbb{R}^{d+\ell}$, i.e., $F_\rho(B)\subset \mathrm{Int}(B)$ for any $\rho\in S$, where S is a region in ρ space [in which, system (4) exhibits synchronization]. Without loss of generality we assume that $B=B_x\times B_y$, i.e., B is a

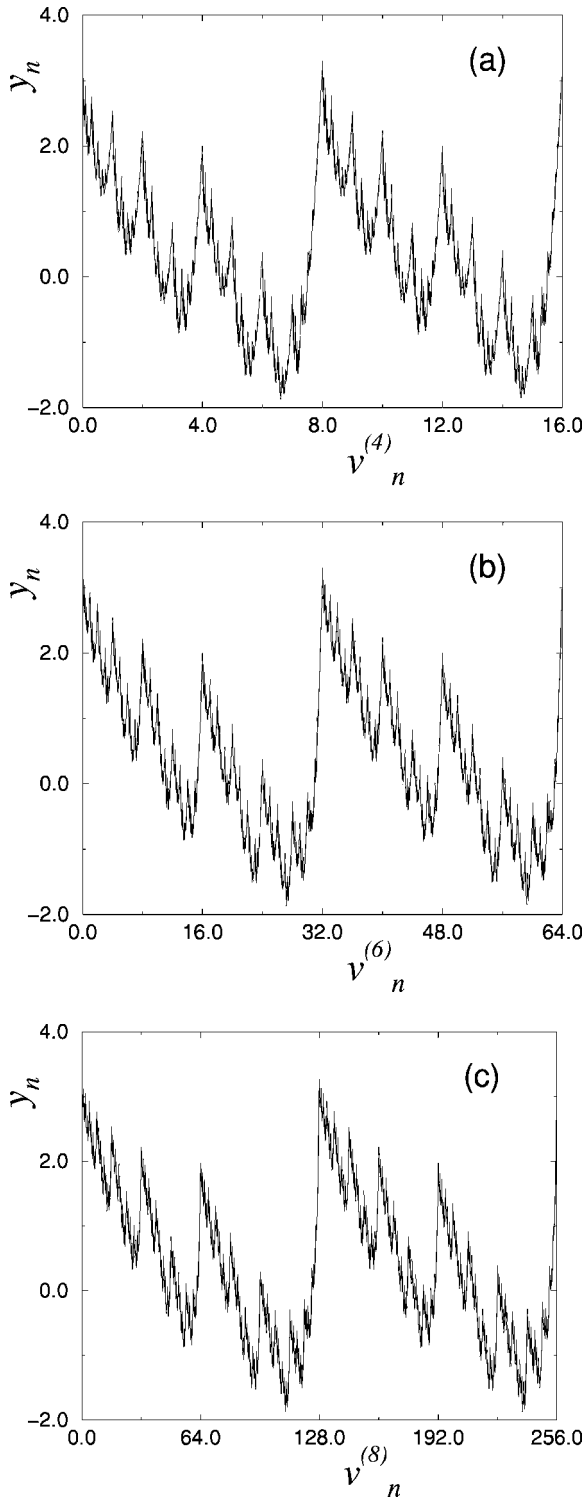

FIG. 5. The synchronization function, shown in Fig. 1, plotted vs a new variable $v_n^{(m)} := I(S_m^i).x_{n-m}^{(1)}$ which contains symbolic information about the driving trajectory. Panel (a) shows the case $m=4$, (b) $m=6$, and (c) $m=8$. Note the changes in the values of the horizontal axes.

rectangle, where B_x (B_y) is a ball in x space (y space). We denote by $\mathcal{A}_\rho$ the maximal attractor in B, i.e., $\mathcal{A}_\rho = \cap_{n=0}^{\infty} F_\rho^n(B)$.

Throughout this section we shall assume that one-to-one globally stable generalized synchronization occurs in B, i.e., condition (5) is satisfied when (x_0,y_0) and $(x_0,\tilde{y}_0)$ are arbitrary points in B.

It was shown in Ref. [23] that under these conditions, there is a continuous functional dependence between x and y components of orbits while the system is in synchronized region. To obtain more detailed characteristics of this functional dependence, we need an additional assumption. Assume that

$$|y_{n+1}-\tilde{y}_{n+1}| \leqslant c|y_n-\tilde{y}_n|, \tag{6}$$

where $c<1$. Of course, parameter c is a function of ρ. For the sake of simplicity, we assume that $c=\rho$. Thus,

$$|y_{n+1}-\tilde{y}_{n+1}| \leqslant \rho|y_n-\tilde{y}_n|, \quad 0<\rho<1. \tag{7}$$

It follows that

$$|g_\rho(x,y)-g_\rho(x,\tilde{y})| \leqslant \rho|y-\tilde{y}| \tag{8}$$

for any (x,y), $(x,\tilde{y}) \in B$. Let us draw attention to the fact that smaller the value of ρ, greater the coupling strength.

Assumption (7) implies that $|y_n-\tilde{y}_n|$ goes to zero exponentially fast, and this fact allows one to prove that function $h: x_n \mapsto y_n$ is Hölder continuous, provided that the functions f and g_ρ have good smooth properties, or at least they are Lipschitz continuous. So we assume that

$$|f(x)-f(\tilde{x})| \leqslant \gamma_+|x-\tilde{x}| \tag{9}$$

and

$$|f^{-1}(x)-f^{-1}(\tilde{x})| \leqslant \gamma_-|x-\tilde{x}|, \tag{10}$$

where $\gamma_-, \gamma_+ \geqslant 1$. Here γ_+ characterizes the rate of divergence of nearby driving trajectories, forward in time and γ_- characterizes their divergence, backward in time. Moreover, we assume that

$$|g_\rho(x,y)-g_\rho(\tilde{x},y)| \leqslant \eta|x-\tilde{x}| \tag{11}$$

for any (x,y), $(\tilde{x},y) \in B$, where $\eta>0$.

The following statement was proved in Ref. [23].

Theorem 1 (Hölder property). Under assumptions (8)–(11), function h is Hölder continuous, i.e., for any $0<\alpha<\alpha_0$ and $x,\tilde{x} \in \mathcal{A}_{\rho,x}$ one has

$$|h(x)-h(\tilde{x})| \leqslant 2a|x-\tilde{x}|^\alpha, \tag{12}$$

where

$$\alpha \leqslant \alpha_0 \equiv \left[1-\frac{\ln(\gamma_+\gamma_-)}{\ln\rho}\right]^{-1} \tag{13}$$

and $a \geqslant a_0$, where $a=a_0$ is the solution of the equation

$$a = \frac{\eta}{\gamma_+-\rho} a^{[\ln(\gamma_+\gamma_-)/\ln\rho]} (\gamma_+\gamma_-)^{1-(\ln|B_y|/\ln\rho)}.$$

Here $|B_y|$ stands for the diameter of B_y. Recall that Hölder exponents quantify the "degree of nondifferentiability."

Our goal is to understand what happens if one tries to study the dependence between y coordinate of the orbit at iteration n and x coordinate at moment $n-m$, for $m>0$. In other words, we are going to study the effect of the "delay" on the functional dependence in the synchronized region. The following result holds.

Theorem 2. Let conditions of Theorem 1 be satisfied and (x_n,y_n), $(\tilde{x}_n,\tilde{y}_n)$ be orbits belonging to $\mathcal{A}_\rho$. Then, for every $\epsilon>0$, there exists $\delta>0$ such that for every pair $x_{n-m},\tilde{x}_{n-m}$ $(|x_{n-m}-\tilde{x}_{n-m}|<\delta)$ one has

$$|y_n-\tilde{y}_n|\leqslant A|x_{n-m}-\tilde{x}_{n-m}|^{\alpha}, \tag{14}$$

where

$$\alpha\leqslant\alpha_0+\beta(\epsilon),\quad \alpha_0\equiv\left[1-\frac{\ln(\gamma_+\gamma_-)}{\ln\rho}\right]^{-1}, \tag{15}$$

and $A\geqslant A_m$, where $\beta(\epsilon)\to 0$ as $\epsilon\to 0$,

$$A_m=\epsilon+\varrho\,\gamma_-^{-m}, \tag{16}$$

and ϱ is a constant independent of m.

Proof. Without loss of generality, we prove estimate (14) for $n=0$. The proof for other values of n is the same. Let $\mathcal{A}_{\rho,x}\equiv\Pi_x\mathcal{A}_\rho$ be the image of $\mathcal{A}_\rho$ under the natural projection Π_x to $\mathbb{R}^d$.

Consider a point $x_0\in\mathcal{A}_{\rho,x}$. Let $x_{-i}\equiv f^{-i}(x_0)$. Given the backward orbit $\{x_{-i}\}_{i=0}^{\infty}$, the dynamics on B_y is defined by the sequence of operators $\{g_\rho(x_{-i},\cdot)\}_{i=0}^{\infty}$ acting on B_y. We define "$\star$" as the following operation:

$$(g_\rho\star g_\rho)(x,y)\equiv g_\rho(f(x),g_\rho(x,y)).$$

We denote by $g_\rho^{\star k}(x,y)$ the result of the operation "$\star$" performed k times (by convention $g_\rho^{\star 0}\equiv g_\rho$). Notice that $g_\rho^{\star k}(x,y)=\Pi_y F_\rho^k(x,y)$.

Consider two points (x_0,y_0) and $(\tilde{x}_0,\tilde{y}_0)$ in the attractor, i.e., $y_0=h(x_0)$, $\tilde{y}_0=h(\tilde{x}_0)$. Their backward orbits, upto time k, are also contained in the attractor. We denote them by

$$(x_{-k},y_{-k}),\ldots,(x_{-1},y_{-1}),(x_0,y_0)$$

and

$$(\tilde{x}_{-k},\tilde{y}_{-k}),\ldots,(\tilde{x}_{-1},\tilde{y}_{-1}),(\tilde{x}_0,\tilde{y}_0).$$

By construction, we have that

$$x_0=f^k(x_{-k}),$$

$$y_0=g_\rho^{\star k}(x_{-k},y_{-k})$$

and

$$\tilde{x}_0=f^k(\tilde{x}_{-k}),$$

$$\tilde{y}_0=g_\rho^{\star k}(\tilde{x}_{-k},\tilde{y}_{-k}).$$

From these equations we can estimate $|y_0-\tilde{y}_0|$. Indeed, triangle inequality yields

$$|y_0-\tilde{y}_0|\leqslant|g_\rho^{\star k}(x_{-k},y_{-k})-g_\rho^{\star k}(x_{-k},\tilde{y}_{-k})| + |g_\rho^{\star k}(x_{-k},\tilde{y}_{-k})-g_\rho^{\star k}(\tilde{x}_{-k},\tilde{y}_{-k})|. \tag{17}$$

The first term on the right can be bounded using the following contracting property of g:

$$|g_\rho^{\star k}(x_{-k},y_{-k})-g_\rho^{\star k}(x_{-k},\tilde{y}_{-n})|\leqslant\rho^k|B_y|, \tag{18}$$

where $|B_y|$ stands for $\mathrm{diam}(B_y)$. The second term can be bounded by

$$|g_\rho^{\star k}(x_{-k},\tilde{y}_{-k})-g_\rho^{\star k}(\tilde{x}_{-k},\tilde{y}_{-k})|\leqslant L_k|x_{-k}-\tilde{x}_{-k}|, \tag{19}$$

where L_k is the Lipschitz constant of $g_\rho^{\star k}(\cdot,y)$. According to Lemma 16 in Ref. [23],

$$L_k\leqslant\frac{\eta}{\gamma_+-\rho}\,\gamma_+^k. \tag{20}$$

Using assumption (10) one gets

$$|x_{-k}-\tilde{x}_{-k}|\leqslant\gamma_-^{k-m}|x_{-m}-\tilde{x}_{-m}|. \tag{21}$$

Putting together these inequalities, one obtains, for all k,

$$|y_0-\tilde{y}_0|\leqslant\rho^k|B_y|+\frac{\eta}{\gamma_+-\rho}\,\gamma_-^{-m}(\gamma_+\gamma_-)^k|x_{-m}-\tilde{x}_{-m}|. \tag{22}$$

For a given ϵ, we fix a small $\sigma\cong\sigma_0(\epsilon)>0$, where $\sigma_0(\epsilon)$ satisfy the relation $[\rho/(\rho+\sigma_0)]^k|B_y|=\epsilon$, and rewrite the first term in Eq. (22) as follows:

$$\rho^k|B_y|=(\rho+\sigma)^k|B_y|\left(\frac{\rho}{\rho+\sigma}\right)^k, \tag{23}$$

then set

$$(\rho+\sigma)^k\cong|x_{-m}-\tilde{x}_{-m}|^{\alpha}. \tag{24}$$

Therefore, using standard logarithmic identity

$$(\gamma_+\gamma_-)^k\equiv G^{k\log_G(\gamma_+\gamma_-)}$$

with $G=|x_{-m}-\tilde{x}_{-m}|$ and formula (24), one can write

$$(\gamma_+\gamma_-)^k\cong|x_{-m}-\tilde{x}_{-m}|^{[\alpha\ln(\gamma_+\gamma_-)/\ln(\rho+\sigma)]}. \tag{25}$$

Let $\alpha=\alpha(\sigma)=[1-\ln(\gamma_+\gamma_-)/\ln(\rho+\sigma)]^{-1}$. Then, Eq. (22) implies

$$|y_0-\tilde{y}_0|\leq\left[\left(\frac{\rho}{\rho+\sigma}\right)^k|B_y|+\frac{\eta}{\gamma_+-\rho}\gamma_-^{-m}\right]|x_{-m}-\tilde{x}_{-m}|^{\alpha(\sigma)}. \tag{26}$$

Thus, if $|x_{-m}-\tilde{x}_{-m}|$ is small enough, then k is large enough because of Eq. (24). Therefore, $[\rho/(\rho+\sigma)]^k|B_y|\leq\epsilon$, $\alpha(\sigma)=\alpha_0+\beta(\epsilon)$, where $\beta(\epsilon)=\ln(\gamma+\gamma)[\ln(1+\sigma_0/\rho)/\ln\rho\ln(\sigma_0+\rho)]$, and the statement of Theorem 2 holds. ■

Hence, we have shown that while the Hölder exponent remains the same as for $m=0$, the Hölder constant A_m, given by formula (16), can be as small as we wish, provided that points on the graph of function h are close enough. In the numerical example presented in Sec. II, the closeness of driving trajectories was achieved by selecting the trajectories with the same symbolic sequence S_m^i.

IV. EFFECTS OF NOISE

The studies presented in Secs. II and III deal with the detectability issues of nondifferentiable (wrinkled) synchronization function when data, acquired from the drive and response systems, are not contaminated by noise. In a realistic situation, external noise is always present in the data. Taking into account the complexity of fine structure, typical for wrinkled synchronization functions, one may expect that even a very small noise in the data ruins the detectability of synchronization. We studied the noise impact using the numerical example considered in Sec. II. We examined how the convergence of the wrinkled function $h^{(m)}$ to a polynomial function is effected by external noise.

The behavior of synchronized systems can be influenced by a noise in many different ways. For example, stochastic forces, applied to the response or drive system, destroy the functional relation between the systems, independent of the complexity of the function shape. The level of destruction in this case will significantly depend upon the dynamical properties of the coupled systems.

To be specific, we will examine only the case when the synchronization function exists, but the data representing this function are contaminated with a noise added to the measurements. Namely, we are dealing with the data $x_n^{(1)}+\xi_n$ and $y_n+\zeta_n$, where $x_n^{(1)}$ and y_n are generated by Eqs. (1) and (2) and the independent noisy components ξ_n and ζ_n are white Gaussian noise with variances σ_D^2 and σ_R^2, respectively. In the numerical analysis, we will also assume that symbolic sequences of driving trajectories are detected correctly.

We found that ξ_n and ζ_n influence the convergence properties differently. To illustrate it, consider, first, the cases when only one source of noise in present. Figure 6 shows the effect of the noise that occurred in the measurements of the response system ($\xi_n=0$ and $\zeta_n\neq0$) for different values of variance σ_R^2. Noise of this type sets a limit on the precision of the function resolution (see Fig. 6). The numerical analysis shows that the limit is $E_{MS}^*\approx\sigma_R^2$. This result is quite predictable. Indeed, noise in the response system destroys the function by scattering points along y variable and makes a thick object (a fuzzy layer) instead of graph $h^{(m)}$. The thickness of the layer is characterized by the level of noise,

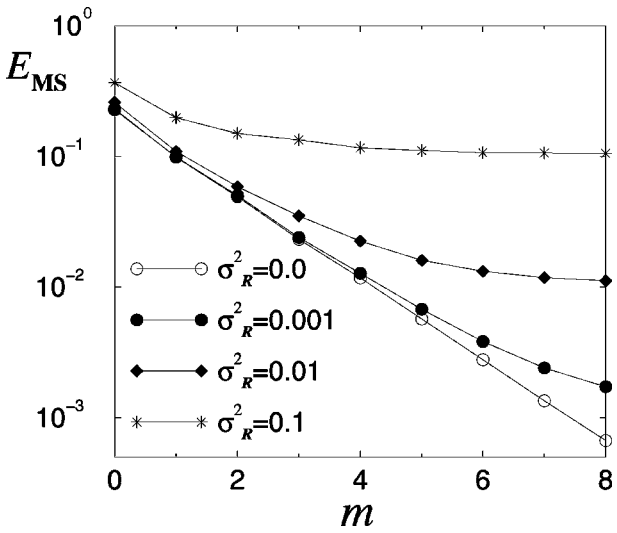

FIG. 6. The dependence of mean squared error of best polynomial fitting function for the attractor points (x_{n-m},y_n) on the mask length m computed for $c=0.7$ and four different values of variance σ_R^2 of the noise added to y_n data.

namely, by σ_R^2. It is clear that the size of the thickness (along y variable) does not change under the transformations applied to the data representing the driving trajectory. Since our method is not designed to locate the function inside this fuzzy layer, we cannot expect the accuracy (in terms of E_{RM}) to be better than σ_R^2.

When noise occurs in the measurements of the driving variable ($\xi_n\neq0$ and $\zeta_n=0$) the conversion process has a different dynamics (see Fig. 7). Now the graph of the function in Fig. 1 is transformed into a thick layer due to scattering of data points along variable x. However, as it follows from Fig. 7, this thickness does not limit the precision of function evaluation. This effect can be understood from the considerations presented in Figs. 1 and 5. Indeed, the increase of trajectory length in the analysis of the function is equivalent to rescaling of the function argument, while the

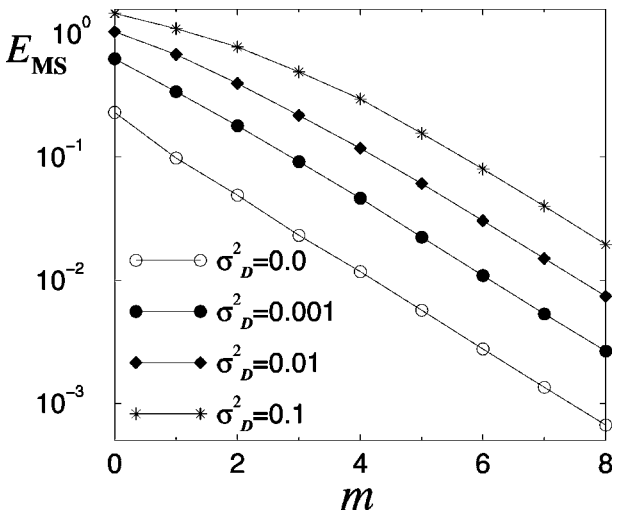

FIG. 7. The dependence of E_{MS} on m computed for $c=0.7$ and four different values of variance σ_D^2 of the noise added to $x_n^{(1)}$ data.

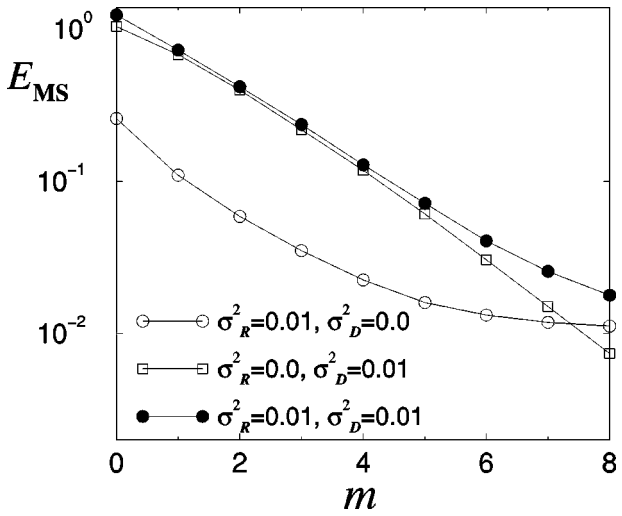

FIG. 8. The dependence of mean squared error of best polynomial fitting function for the attractor points (x_{n-m}, y_n) on the trajectory length m computed for three different n.

overall shape of the function does not change (see Fig. 5). While the interval of the argument values increases with the trajectory length, as 2^m, the x size of the thick layer remains unchanged. As a result, an increase of m, in this case, improves the precision of function detection.

The effects induced by additive noise in the data are summarized in Fig. 8 where the dependence of E_{MS} on m is shown for three different situations of noise ($\xi_n=0$, $\zeta_n \neq 0$), ($\xi_n \neq 0$, $\zeta_n=0$), and ($\xi_n \neq 0$, $\zeta_n \neq 0$). These plots are computed for the coupling strength $c=0.7$. The results indicate that if the level of noise in the data is small, a nondifferentiable function is detectable with some accuracy limited by the noise variance.

In this analysis we assumed that the symbolic sequence representing the driving trajectory is detected correctly. We expect that if the symbolic sequence contains errors then the modified function $h^{(m)}$ can be severely damaged and the improvement of function detection can fail. We believe that the use of a noise reduction technique can be very beneficial for correcting of errors in the symbolic sequence.

V. CONCLUSIONS

A simple numerical example and rigorous theoretical analysis show that, despite complex shapes of nondifferentiable synchronization functions, the existence of such a function can be detectable in practical situation. This can be achieved by considering this function not as a function of the current state of driving system, but as a function of the state, in which the driving system has been a few steps early. Thanks to the contracting properties caused by the dissipation in the driving system, the nearby trajectories dispersed far away from each other in the previous times. This effect can be used as a ''magnifying glass'' in the detection of nondifferentiable synchronization function that contains multiple wrinkles and cusps. It is shown that, although the ''magnified'' function in this analysis remains nondifferentiable, the amplitude of these wrinkles and cusps gets smaller as the delay increases.

The results presented in this paper are in agreement with the recent study on detection of generalized synchrony made by He, Zheng, and Stone [27]. Their study is based on a different technique that involves the analysis of drive and response trajectories in the embedded phase spaces, and takes into account p preimages for each trajectory point. The use of the preimages in this case also acts as a magnifying glass in detecting of the wrinkled synchronization function.

In the example considered in Sec. II, the synchronization function depends only on the $x^{(1)}$ variable, which is the coordinate that always represents a stable direction in **x**. Stable and unstable directions in **x** space in this driving system are fixed and do not dependent on **x**. Therefore, the differential of this map is a constant matrix. In a more general situation this is not the case, and the synchronization function must depend on both stable and unstable coordinates. Nevertheless, it is possible to understand (although it is not so simple to prove) that the dependence on the unstable coordinate is nonessential in the hyperbolic situations. The simplest way to be convinced is to remember that for hyperbolic attractor there exists a local Hölder-continuous change of variables, such that in new variables the stable and unstable directions are along the coordinate lines (planes) and the situation becomes very similar to the example considered.

We examined the influence of external noise on the function improvement. We found that noise in the data acquired from the response system sets a limit for the accuracy of the function approximation and, as a result, after some critical value of m, further increase of delay becomes useless.

To conclude, we would like to emphasize that although we apply our study to the theory of chaos synchronization, the data analysis method and theory developed here can be useful for other applications. Such applications include prediction of chaotic dynamical behavior in time and space and other studies associated with various types of prediction. The use of hybrid, ''continuous-symbolic'' representation of the chaotic trajectories enables one to take into account additional information about the trajectory in a compact way.

It is clear that, since improvement of the function detectability relies on increasing of resolution in the analysis of chaotic attractor in the driving system, each step in the improvement requires a larger number of points to be available for the analysis. As a result, detectability of the function can be limited not only by a noise in the data, but also by the limited number of data points.

ACKNOWLEDGMENTS

The authors are grateful to A. Cordonet, J. Urias, L.S. Tsimring, H.D.I. Abarbanel, and M.I. Rabinovich for stimulating discussions. This work was supported in part by a grant from the University of California Institute for Mexico and the United States (UC MEXUS) and the Consejo Nacional de Ciencia y Tecnologia de México (CONACYT). N.R. was sponsored in part by U.S. Department of Energy (Grant No. DE-FG03-95ER14516) and the U.S. Army Research Office (MURI Grant No. DAAG55-98-1-0269). V.A was partially supported by CONACyT Grant No. 36445-E.

[1] L. Glass and M.C. Mackey, *From Clocks to Chaos: the Rhythms of Life* (Princeton University Press, Princeton, 1988), p. 248.
[2] N. Minorsky, *Nonlinear Oscillations* (R.E. Krieger, Huntington, 1974), p. 714.
[3] I.I. Blekhman, *Synchronization in Science and Technology* (ASME Press, New York, 1988), p. 255.
[4] A. Pikovsky, M. Rosenblum, and J. Kurths, *Synchronization: A Universal Concept in Nonlinear Science* (Cambridge University Press, Combridge, 2002), p. 500.
[5] E. Mosekilde, Yu. Maistrenko, and D. Postnov, *Chaotic Synchronization: Applications to Living Systems* (World Scientific, Singapore, 2002), p. 440.
[6] S. Boccaletti, J. Kurths, G. Osipov, D.L. Valladares, and C.S. Zhou, Phys. Rep. **366**, 1 (2002).
[7] V. Afraimovich, N.N. Verichev, and M.I. Rabinovich, Radiophys. Quantum Electron. **29**, 747 (1986).
[8] H. Fujisaka and T. Yamada, Prog. Theor. Phys. **69**, 32 (1984).
[9] L.M. Pecora and T.L. Carroll, Phys. Rev. Lett. **64**, 821 (1990).
[10] N.F. Rulkov, M.M. Sushchik, L.S. Tsimring, and H.D.I. Abarbanel, Phys. Rev. E **51**, 980 (1995).
[11] L.M. Pecora, T.L. Carroll, and J.F. Heagy, Phys. Rev. E **52**, 3420 (1995).
[12] L. Kocarev and U. Parlitz, Phys. Rev. Lett. **76**, 1816 (1996).
[13] N.F. Rulkov, V.S. Afraimovich, C.T. Lewis, J.-R. Chazottes, and A. Cordonet, Phys. Rev. E **64**, 016217 (2001).
[14] A. Pikovsky, M. Zaks, M. Rosenblum, G. Osipov, and J. Kurths, Chaos **7**, 680 (1997).
[15] M.A. Zaks, E.H. Park, M.G. Rosenblum, and J. Kurths, Phys. Rev. Lett. **82**, 4228 (1999).
[16] B. van der Pol, Philos. Mag. **3**, 65 (1927).
[17] A.A. Andronov and A. A Witt, Arch. Elektrotech. (Berlin) **16**, 280 (1930).
[18] H.D.I. Abarbanel, N.F. Rulkov, and M.M. Sushchik, Phys. Rev. E **53**, 4528 (1996).
[19] J. Stark, Physica D **10**, 163 (1997).
[20] B.R. Hunt, E. Ott, and J.A. Yorke, Phys. Rev. E **55**, 4029 (1997).
[21] K. Josić, Phys. Rev. Lett. **80**, 3053 (1998).
[22] J. Stark, Ergod. Theory Dyn. Syst. **19**, 155 (1999).
[23] V. Afraimovich, J.-R. Chazottes, and A. Cordonet, Discrete Contin. Dyn. Syst., Ser. B **1**, 421 (2001).
[24] P. So, E. Barreto, K. Josić, E. Sander, and S.J. Schiff, Phys. Rev. E **65**, 046225 (2002).
[25] E. Barreto, K. Josić, C. Morales, E. Sander, and P. So, Chaos **13**, 151 (2003).
[26] V. Afraimovich, A. Cordonet, and N.F. Rulkov, Phys. Rev. E **66**, 016208 (2002).
[27] D. He, Z. Zheng, and L. Stone, Phys. Rev. E **67**, 026223 (2003).